technical memorandum Daresbury Laboratory

DL/CSE/TM14

A PARTICLE IDENTIFIER FOR LIGHT IONS

by

J.B.A. ENGLAND, University of Birmingham;

and

M.M. PRZYBYLSKI and G. SALVINI, Daresbury Laboratory

AUGUST, 1981

Science Research Council

Daresbury Laboratory

Daresbury, Warrington WA4 4AD

A PARTICLE IDENTIFIER FOR LIGHT IONS

by

J.B.A. ENGLAND
Department of Physics, University of Birmingham

and

M.M. PRZYBYLSKI and G. SALVINI
Daresbury Laboratory

ABSTRACT

The fast analogue Particle Identifier for light ions, utilising the E and ΔE signals from a detector telescope as inputs, has been designed for the Nuclear Structure Facility at the Daresbury Laboratory.

The identifier which is of integrated circuit-construction, is based on the AD.429B multiplier. It is capable of generating three functions: a first order and two second order identification functions.

SCIENCE AND ENGINEERING RESEARCH COUNCIL

DARESBURY LABORATORY

1. INTRODUCTION

When fast charged particles interact with nuclei, their reaction products can contain many different particle types. The problem facing the experimenter is to obtain a mass and charge identification of these emerging particles. This must be done so that their angular distribution may be unambiguously obtained and hence the effects of nuclear forces examined.

Arrays of telescopes made of thin 'ΔE' detectors mounted in front of an 'E' stopping detector, are positioned around the target under high vacuum in the 'scattering chamber', to provide information on the types of particles and their distribution in space.

The two signals, E and ΔE, generated in a telescope are the variables from which an identifying function proportional to MZ^2 may be obtained, where M and Z are the mass and atomic number of the particle stopped in the detector. The value of this function is constant for particles of a particular type, independent of their energies.

The present PI (Particle Idfentifier) will provide on-line mass and charge identification in experiments at the Daresbury Laboratory Nuclear Structure Facility, for detected particles up to boron and charge identification for elements up to fluorine.

The unit has the following salient features:

(a) It provides a fast first or second order approximation of the expanded identification function.

(b) It can be set up easily from the E and ΔE inputs, without need for an on-line adjustments.

(c) It is an all integrated circuit analogue unit in a single width NIM module.

2. PRINCIPLE OF OPERATION

The generated identification function in the PI is based on the Bethe-Bloch formula for energy loss from a charged particle of kinetic energy E, passing through a given material[1] i.e.

$$\frac{dE}{dx} = C_1 \frac{MZ^2}{E} \ln \frac{C_2 M}{M} \quad (1)$$

where : C_1 and C_2 are physical constants dependent on the detector material, in our case Silicone.

$\frac{dE}{dx}$ is the ΔE loss in the first detector of the telescope.

and E is the initial particle energy.

The equation can be re-arranged in terms of MZ^2, mass and charge:

$$MZ^2 = \frac{1}{C_1} * \Delta E * E * \frac{1}{\left(\ln \frac{C_2 E}{M}\right)} \quad (2)$$

which can be expressed as[2]:

$$MZ^2 \alpha \Delta E\left(E + K_0 - K_1\Delta E + K_2\Delta E^2 - K_3\Delta E^3 + \ldots\right) \quad (3)$$

Taking into consideration the semi-empirical evolution of the coefficients carried out by England[2] or Gupta[3] over an energy range from 5 to 100 MeV, from protons to alpha particles, the above expansion can be re-written in the form:

$$MZ^2 \tilde{\alpha} \Delta E\left(E_T - K_1\Delta E + K_0\right) \quad (4)$$

where : $K_0 \tilde{=}$ 7.0 and it has the dimension of energy

$K_1 =$ 0.5 is dimensionless

and $E_T = E' + \Delta E$

The value of K_0 depends critically on a theoretical fit to the lowest energy data[4]. Recent experiments to determine K_0 have shown that it

should be less than 7.0. However, the values of these constants depend on the gains or dispersions in the E and ΔE channels in the following ways:

$$K_1 = \frac{\Delta E \text{ Dispersion}}{E \text{ Dispersion}} \quad (5)$$

and

$$K_0 = \frac{1}{E \text{ Dispersion}} \quad (6)$$

The following approximation $(E_T - K_1\Delta E) \tilde{=} (E' + K_1\Delta E)$ enables two types of identification functions; one as a function of ET and ΔE the other in E' and ΔE.

The PI provides three functions: a first order

$$F_1 = (E_T + K_0)\ \Delta E \quad (7)$$

and two second order:

$$F_2 \equiv \left([E_T - 0.5\ \Delta E] + K_0\right)\ \Delta E \quad (8)$$

$$F_3 = \left([E' + 0.5\ \Delta E] + K_0\right)\ \Delta E \quad (9)$$

It also has two independently adjustable dispersion gain controls from 1 to 11 (MeV)/V, for E and 0 to 10 (MeV)/V for ΔE, giving a dynamic acceptance of up to 100 MeV equivalent signals from the solid state detecors. The unit will accept up to 10 V, 0.5 µs shaped input pulses and it provides both unipolar and bipolar outputs. An E_T output is also provided. A block diagram of the PI is shown in fig.1.

At the heart of the unit is a four quadrant multiplier, with a wide bandwidth full power response, to give low distortion. It provides the $E^*\Delta E$ and the second order product $\pm K_1\Delta E^2$ in the F_2 and F_3 functions.

The linear factor $K_0\Delta E$ is summed after the multiplier block in E_4, fig.4 which also provides a variable gain for the linear and bipolar outputs.

All the dispersion corrections are done in the ΔE channel relative to E' or E_T.

The input buffer E_{12} and E_{13} in the ΔE channel, drives the E dispersion factor switch and associated helipot in an attenuating mode and the ΔE dispersion factor and switch in an amplifying mode. The K_0 linear fraction is also generated after the E dispersion attenuator. Amplifiers E_{14} and E_7 provide the $\pm K_1\Delta E$ which is summed in E_2 with the incoming inverted signal E to generate the second order correction term $\pm 0.5\ \Delta E^2$ in F_2 and F_3 after the multiplier.

3. CIRCUIT DESCRIPTION

The complete formuli with the inclusion of the Dispersion Factors and output gain selection provided by the PI are:

$$F_1 = \frac{G}{10}\left[E_T + \frac{K_0}{DF_E}\right]\Delta E \qquad (10)$$

$$F_2 = \frac{G}{10}\left[\left(E_T + \frac{DF_{\Delta E}}{DF_E} K_1\ \Delta E\right)\Delta E + \frac{K_0}{DF_E}\Delta E\right] \qquad (11)$$

$$F_3 = \frac{G}{10}\left[\left(E' + \frac{DF_{\Delta E}}{DF_E} K_1\ \Delta E\right)\Delta E + \frac{K_0}{DF_E}\Delta E\right] \qquad (12)$$

where DF_E and $DF_{\Delta E}$ are dispersion factors of E and ΔE signals. The input signals required by the PI are 0.5 to 2.0 μs shaped pulses, as from the Ortec 572 type amplifier. The circuit diagram and specifications of the unit are given in fig.4 and in appendix A respectively.

An operational amplifier, should have a bandwidth at least 5 times the centre frequency of the pulse used, to give an error in amplitude of less than 2%. On the other hand any tendency to overshoot should be minimised. The delays through the different paths in the circuit should be matched so that linearity is maintained after multiplication and summing.

The chosen amplifier is the PH1322 with a 1.6 MHz full power bandwidth. The PH1322 is configured as a stable and fast inverter and its low drift characteristic reduces the offset errors at the input of the multiplier block. The inverting and summing stages have been equalised with an input phase compensation that extends their dynamic range to above 1.5 MHz (fig.2). The delay through the amplifier is 40 ns.

An error is introduced in the summing of two semi-Gaussian pulses, which are not perfectly coincident in time. In the path, where K_1DE is generated, because of the extra delay introduced by E_{14} and E_7 amplifiers relative to the input E signal, a correction must be made to restore a true sum in E_2.

A wider bandwidth device, the LH0024, was selected for the X5 amplifier E_{14}. It was designed with a low drift feedback network and has a 20 ns longer propagation time than the inverting PH1322 stage. An increase in amplitude was made in $K_1\Delta E$ chain to compensate for the effect of difference in time of $K_1\Delta E$ with E and ΔE. That way, pulse distortion created by the delay, is partially compensated, in the product of the semi-Gaussian inputs in the multiplier.

The ΔE non-inverting input buffer $E_{12\text{-}13}$ has to drive the low impedance dispersion controls, to keep the loading error at the helipots below 1%. A PH1322 amplifier followed by an MC1438R buffer enclosed in the same feedback loop, with compensating networks were used to achieve a full power response to over 1.5 MHz.

The same pair of IC's are used for the inverting output configurations to obtain a controlled output impedance with good gain stability.

The bipolar output is obtained in E_{10-11} with a single stage passive RC differentiation for a 0.5 μs shaped input pulse. The differentiation was designed to give equality of peak amplitude between input and output for 0.5 μs shaped pulses.

The 429B Analogue Devices multiplier with a full power bandwidth of 2 MHz, was set up for minimum offset and feedthrough for 3V, 0.5 μs shaped pulses. The error introduced by the 429B is below 1%.

The unit, with an all d.c. path, is sensitive to offsets at the input of the multiplier, as a source of error in the generated function.

The fraction $K_0\Delta E$ gives the largest term of the functions for low values of E and ΔE.

By selecting a low output impedance for the ΔE input buffer and for the dispersion controls, the K_0 fraction could be set to better than ± 0.5%. The circuit diagram of the PI is shown in fig.4 and a complete unit is shown in fig.3.

4. TESTS AND PERFORMANCE

4.1 Dynamic Test of the 429B Analogue Multiplier

The accuracy of the 429B analogue multiplier degrades above 100 kHz.

A dynamic test with 0.5 μs shaped input pulses was performed. After adjustment of the offset and feedthrough, the same pulse was applied to both inputs of the multiplier. The output was measured for a 0.01 V to 10 V range of input voltages. Deviation from a square law characteristic is shown in fig.5.

4.2 Dynamic Test of the PI

For test purposes the PI is considered as an analogue computer capable of generating the three functions F_1, F_2 and F_3. The putput was measured as a function of E, with ΔE as a parameter.

A series of error curves from computed values are shown in fig.6 for the three functions F_1, F_2 and F_3. Errors are expressed as a percentage of reading. A block diagram of the test circuit is shown in fig.7.

4.3 Temperature Tests

Three tests were carried out to check the temperature characteristic of the PI in the range 20-50°C.

The first was a cycling test from switch-on to 50°C and back again to 20°C. This was done by recording the output of the PI set to F1 = 6 V while varying the temperature (fig.8a).

The second test was carried out for F_1, F_2 and F_3 with E and ΔE inputs set to 1 volt (fig.8b).

The drift was 0.5 mV/°C and was linear throughout the range from 10 to 50°C.

4.4 Performance

The PI was tested with 3He and 4He charged particle beams from the Radial Ridge AVF cyclotron of the Department of Physics, University of Birmingham.

On the first test the set up was as follows: 33 MeV $^3He^+$ polarized beam on 56Fe target at 62.5° lab. The E discriminator was set at 0.5 MeV and the ΔE at 0.25 MeV. The PI was set to F_3 and the output gain to X4, while the dispersion factors DF_E and $DF_{\Delta E}$ were both set at 4.3 MeV/V.

Mass and Energy spectra are shown in figs.9, 10 and 11. The mass spectrum shows very good separation of 3He and 4He.

On the second run α sources were placed in front of the detectors in the telescope to optimize the dispersion factors.

The setup was as follows: 25 MeV, ^4He on a carbon backed titanium target at 30° lab. The target was: $^{12}C(\alpha,\alpha)$, $^{16}O(\alpha,\alpha)$, $^{50}Ti(\alpha,\alpha)$ and

$^{181}Ta(\alpha,\alpha)$. The PI was set at F3 and the energy spectrum was accumulated from the ET output of the unit. The resolution of the energy spectrum was 0.45% (fig.13). The mass spectrum was good as may be seen (fig.12).

A number of runs were taken with different setting of DF_E leaving constant the $DF_{\Delta E}$. Because of the high accuracy of the unit, an interesting fact emerged; the setting for the best resolution of an energy spectrum is different from the setting for the best 'mass spectrum'.

This implies that the empirical K_0 factor differs from the value of $K_0 = 7.00$.

The K_0 was changed to a new value of $K_0 = 6.0$, keeping the Dispersion Factor calibrated with the α source. As seen from the graphs figs.14 and 15 a factor of 3 improvement in E_T resolution was obtained, while the mass spectrum remains unchanged.

5. CONCLUSIONS

A new and improved version of a PI has been designed and tested. The unit met its target specifications. The high accuracy and stability of the unit in generating the analogue functions allows the confirmation of the experimental observations that K_0 should be less than 7.0 as suggested from fits to the theoretical range energy data by Skyrme[4-6].

The functions generated by the unit perform well for ions up to boron isotopes and give good charge separation up to fluorine.

Improvements could be made by the addition of the third and fourth order terms in the identifying function to give complete isotope identification up to oxygen.

ACKNOWLEDGEMENTS

We wish to thank Professor G.C. Morrison and the Nuclear Structure Group of Birmingham for allowing the experimental run on the unit and G. Hughes of Daresbury Laboratory for encouragement during the project.

A special thanks to D. Newton who provided the assistance during the experimental run and provided the software for the graph plotting routines.

REFERENCES

1. M.S. Livingston and H.A. Bethe, Rev. Mod. Phys. 9, (1937) 245.
2. J.B.A. England, Technique in nuclear structure physics, Ch5 (London: Macmillan, 1973)
3. S.K. Gupta, Nucl. Instr. and Meth. 92, (1971) 33.
4. D.J. Skyrme, Nucl. Instr. and Meth. 57, (1967) 61.
5. J.B.A. England, Nucl. Instr. and Meth. 106, (1973) 45.
6. J.B.A. England, private communication (1980).

APPENDIX A

Particle Identifier for Light Ions

(Provisional Specification)

Inputs : E and ΔE, d.c. or a.c. coupled (front panel selectable), 0 to 10 V input range. Impedance: 1kΩ ± 1% on d.c. 1kΩ ± 1% in series with capacitor on a.c.

The ratings are for 0.5 μs shaped pulses from ORTEC 572, 451 or 471 amplifiers.

Outputs : O/P1

Positive, unipolar, d.c. coupled, 0 to 10 V.

output impedance 50 Ω V 5%

Front panel selectable functions

1) $F_1 = C(E_T + K_0)\Delta E$

2) $F_2 = C(E_T - 0.5\Delta E + 7.0)\Delta E$

3) $F_3 = C(E' + 0.5\Delta E + 7.0)\Delta E$

where $E_T = E' + \Delta E$

E_T = total energy

E' = stopping energy

ΔE = energy in dE/dx detector

C = constant.

O/P2

Positive-going bipolar, 0 to 10 V at 0.5 μs shaping, generated by single stage pasice RC differentiation of O/P1.

output impedance 50 Ω ± 5%.

O/P3

Positive unipolar $E_T = E' + \Delta E$ signal,

Gain unity ± 3% at 5 V output

output impedance 50 Ω ± 5%.

Output Gain :	x1, x2, x4, x8 ± 10%
D.c. Adjust :	Front panel multiturn potentiometer giving a ± 1 V range of adjustment.
Integral Non-Linearity:	Less than ± 2% of full scale over a 1 V to 10 V range of ΔE signals for 0 < E < 10 V), for 0.5 μs shaped pulses from ORTEC 572, 451 or 471.
Gain Stability:	± 10mV/°C
D.c. Drift:	± 10 mV/°C
Dimensions:	Single width NIM
Power:	± 24 V
Connectors:	E, ΔE, O/P$_1$, O/P$_2$, O/P$_3$ - BNC front panel

FIGURE CAPTIONS

Fig.1	Particle identifier block diagram.
Fig.2	Typical inverting stage with compensation.
Fig.3	Photograph of the complete unit.
Fig.4 a & b	Particle identifier schematic circuit diagrams.
Fig.5	Accuracy of the analogue multiplier block 429B with 0.5 μs shaped input pulses.
Fig.6	Error curves of the PI for the three functions F_1, F_2 and F_3.
Fig.7	Set-up to measure deviation in the PI from computed values.
Fig.8	Temperature performance of the PI.
Fig.9	Energy spectrum before identification.
Fig.10	Identified ^{3}He and ^{4}He mass spectra.
Fig.11	3D identified mass spectra from P to ^{3}He.
Fig.12	P, D and T mass spectrum.
Fig.13	Resolution of the energy spectrum by the PI.
Fig.14	Improved energy resolution with K_0 = 6.0
Fig.15	Mass spectrum with K_0 = 6.0

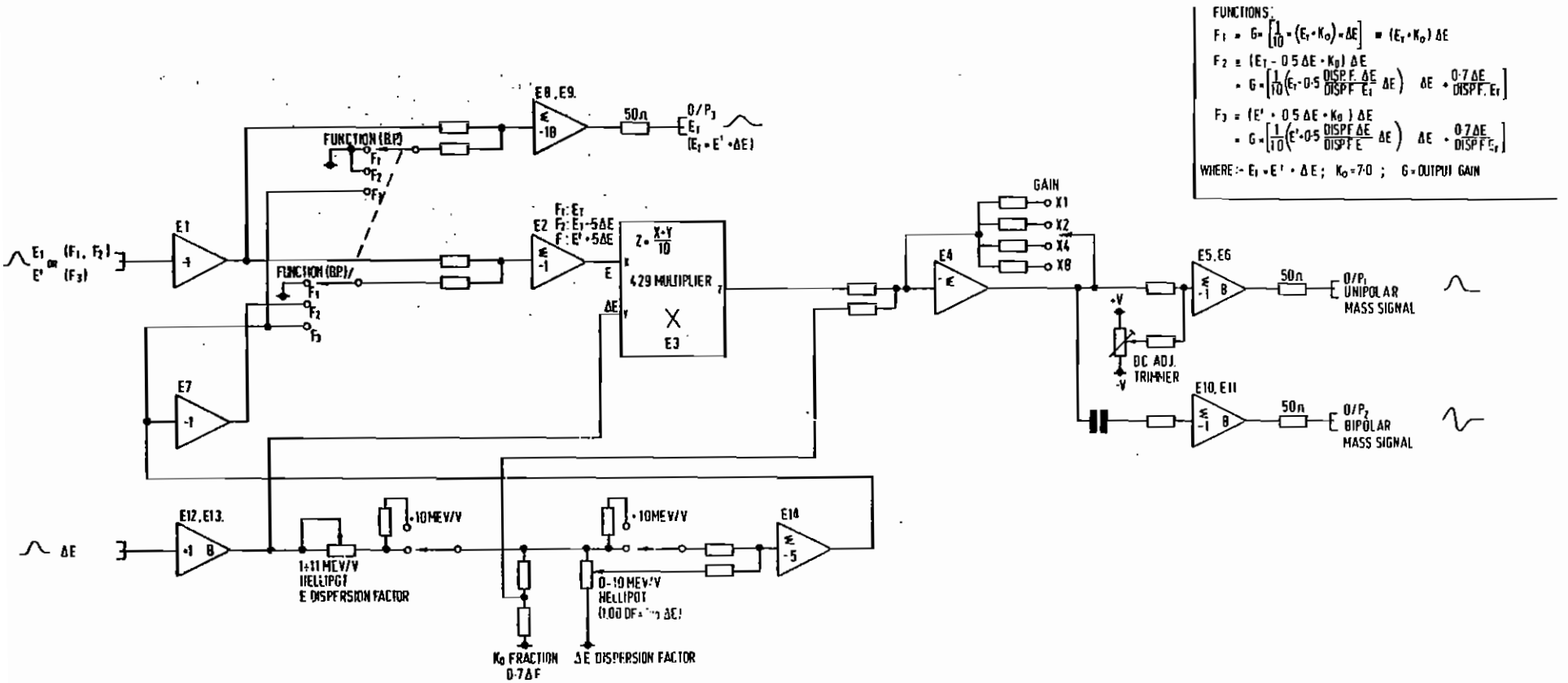
FUNCTIONS:
F1 = G = [1/10 (E1 + K0) ΔE] = (E1 + K0) ΔE
F2 = (E1 - 0.5 ΔE + K0) ΔE
= G = [1/10 (E1 - 0.5 DISP.F. ΔE / DISP.F. E1 ΔE) ΔE + 0.7 ΔE / DISP.F. E1]
F3 = (E' + 0.5 ΔE + K0) ΔE
= G = [1/10 (E' + 0.5 DISP.F. ΔE / DISP.F. E ΔE) ΔE + 0.7 ΔE / DISP.F. E1]
WHERE :- E1 = E' + ΔE ; K0 = 7.0 ; G = OUTPUT GAIN
E8, E9.
50Ω
O/P3
E1 = E' + ΔE
FUNCTION (B.P.)
F1
F2
F3
E1
E1 OR E' (F1, F2) (F3)
E2
F1: E1
F2: E1 - 5ΔE
F: E' + 5ΔE
Z = X·Y / 10
429 MULTIPLIER
X
E3
E
ΔE
GAIN
X1
X2
X4
X8
E4
E5, E6
O/P1
UNIPOLAR
MASS SIGNAL
+V
-V
DC ADJ.
TRIMMER
E7
E10, E11
O/P2
BIPOLAR
MASS SIGNAL
E12, E13.
ΔE
10 MEV/V
1-11 MEV/V
HELLIPOT
E DISPERSION FACTOR
10 MEV/V
E14
0-10 MEV/V
HELLIPOT
(100 DISP. ΔE)
K0 FRACTION
0·7 ΔE
ΔE DISPERSION FACTOR

Fig.1

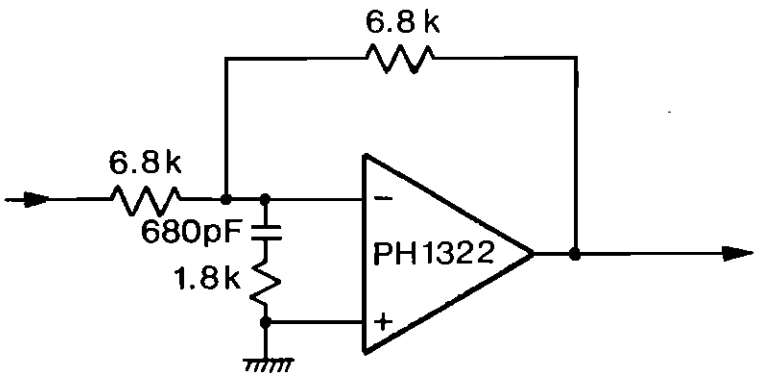

Fig. 2

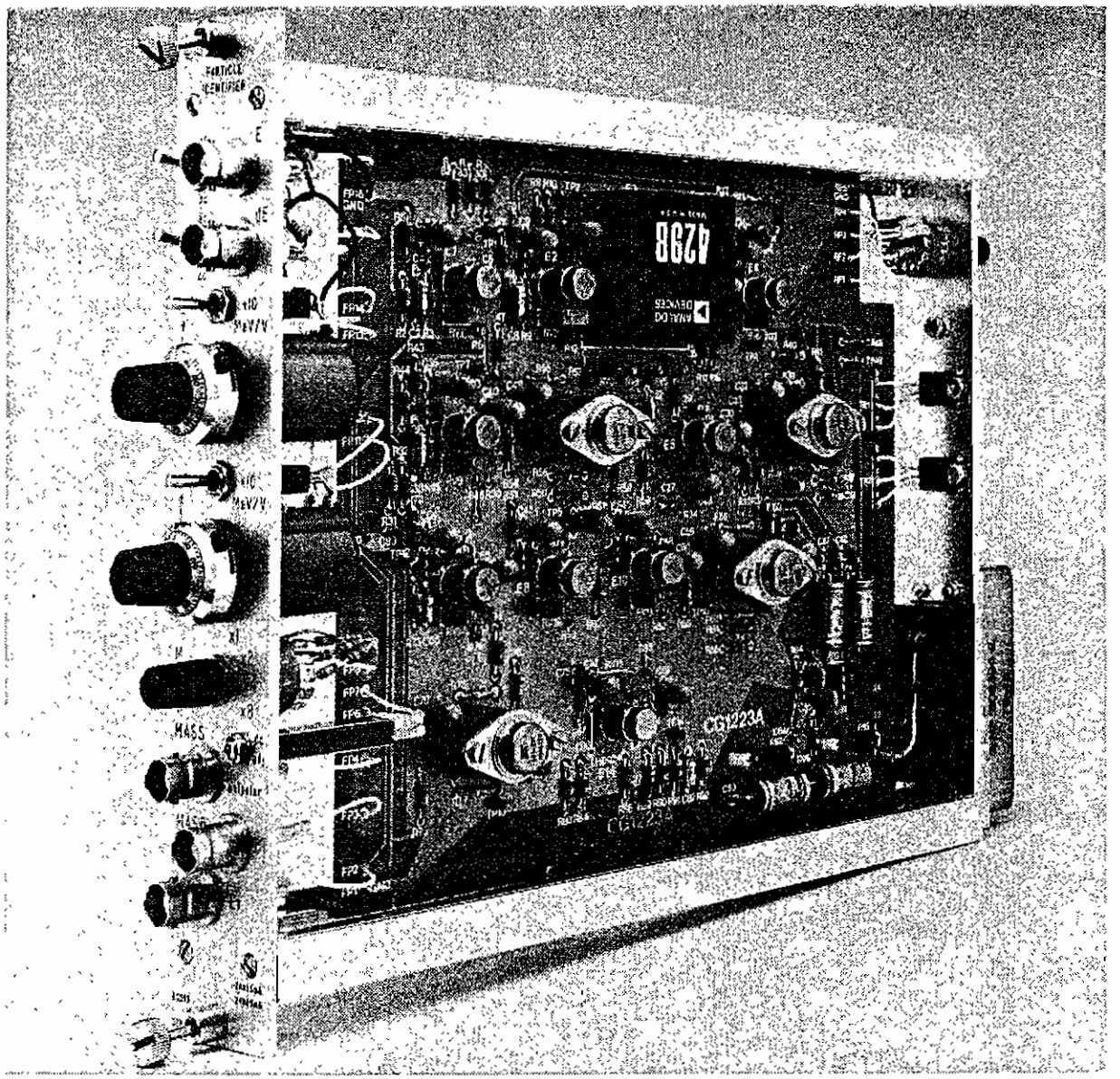

Fig.3

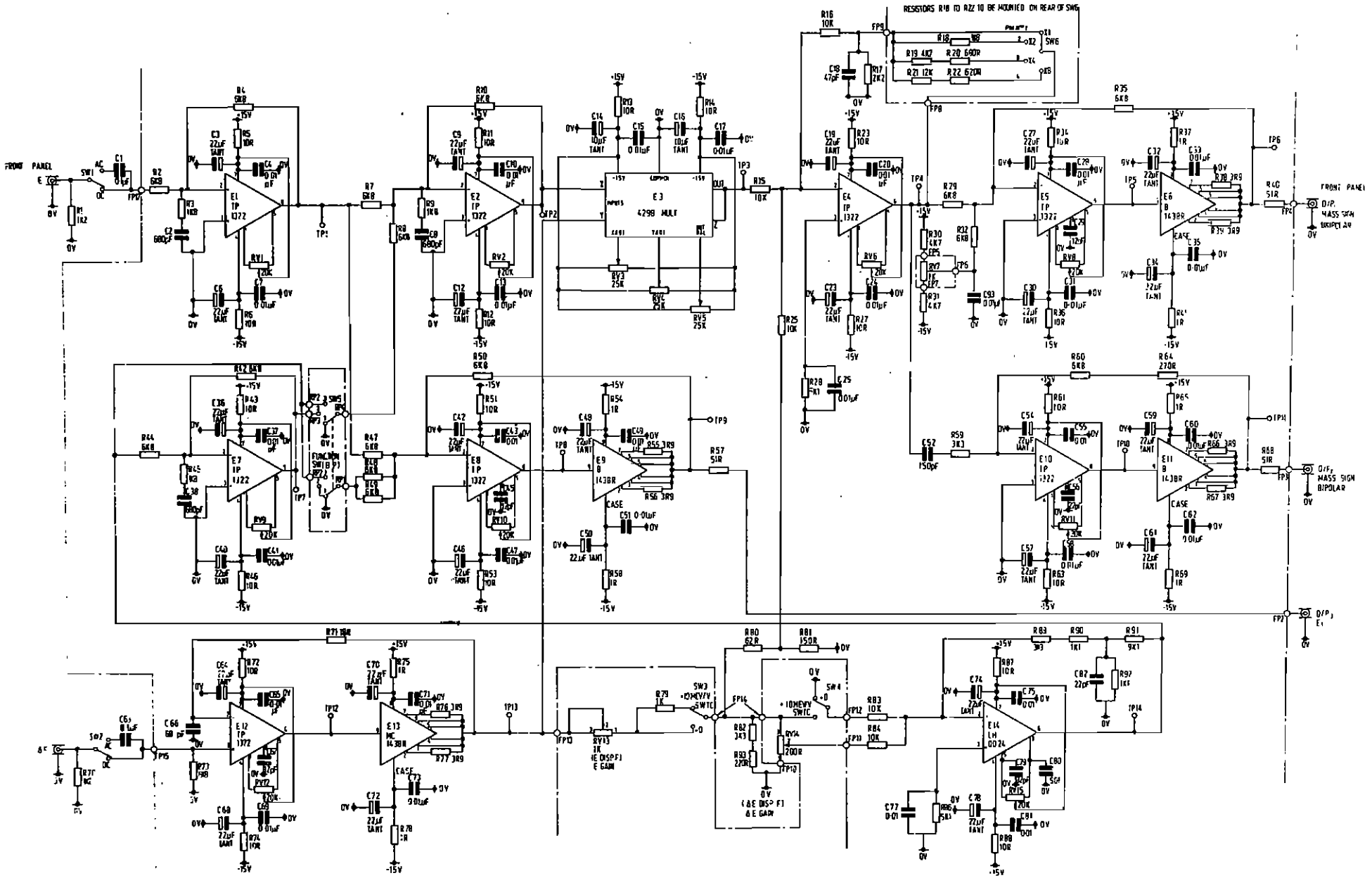

Fig. 4a

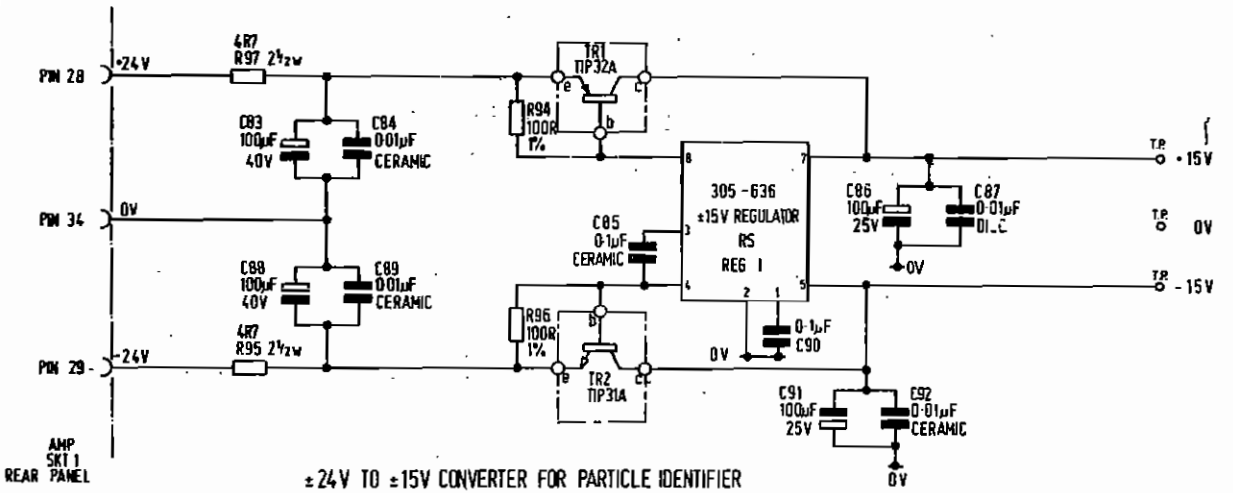

±24V TO ±15V CONVERTER FOR PARTICLE IDENTIFIER

Fig.4b

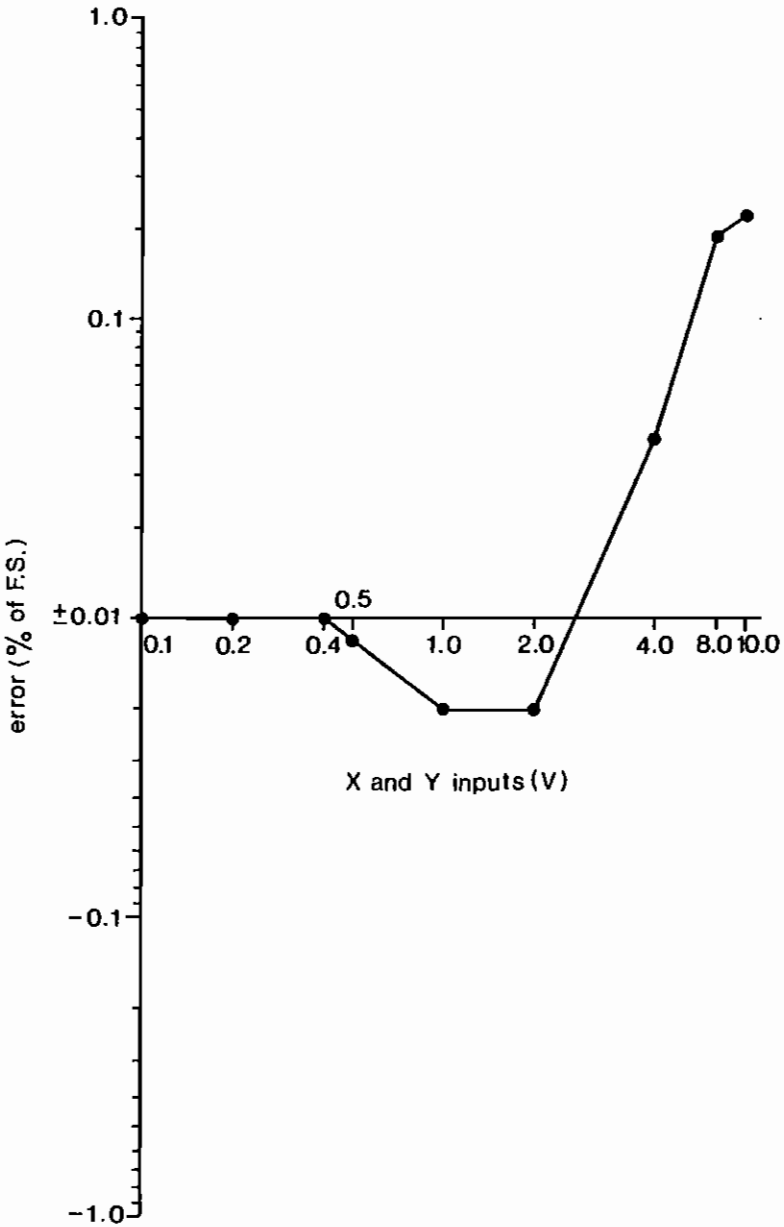
1.0
0.1
±0.01
−0.1
−1.0
error (% of F.S.)
0.1
0.2
0.4
0.5
1.0
2.0
4.0
8.0
10.0
X and Y inputs (V)

Fig. 5

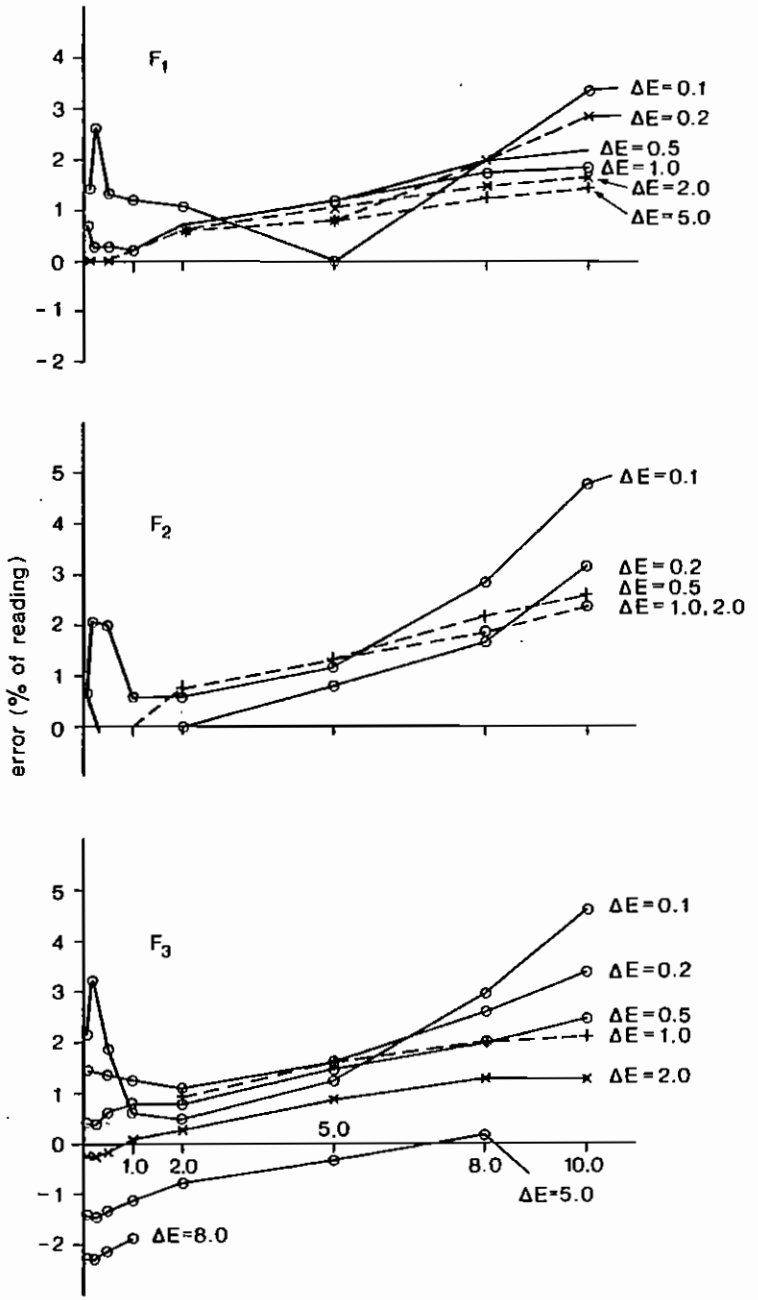
F1
ΔE=0.1
ΔE=0.2
ΔE=0.5
ΔE=1.0
ΔE=2.0
ΔE=5.0
F2
ΔE=0.1
ΔE=0.2
ΔE=0.5
ΔE=1.0, 2.0
F3
ΔE=0.1
ΔE=0.2
ΔE=0.5
ΔE=1.0
ΔE=2.0
ΔE=5.0
ΔE=8.0
5.0
1.0
2.0
8.0
10.0
error (% of reading)
E input (V)

Fig. 6

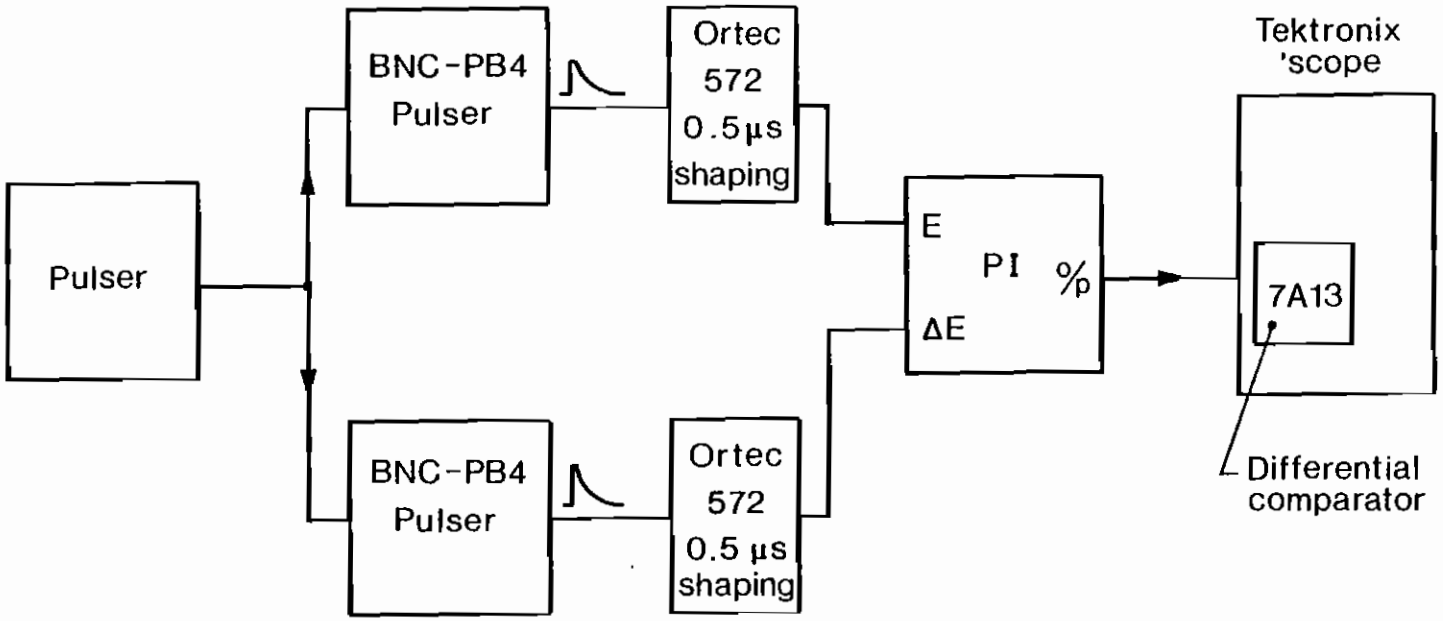
Pulser
BNC-PB4
Pulser
BNC-PB4
Pulser
Ortec
572
0.5µs
shaping
Ortec
572
0.5 µs
shaping
E
PI %
ΔE
Tektronix
'scope
7A13
Differential
comparator

Fig 7

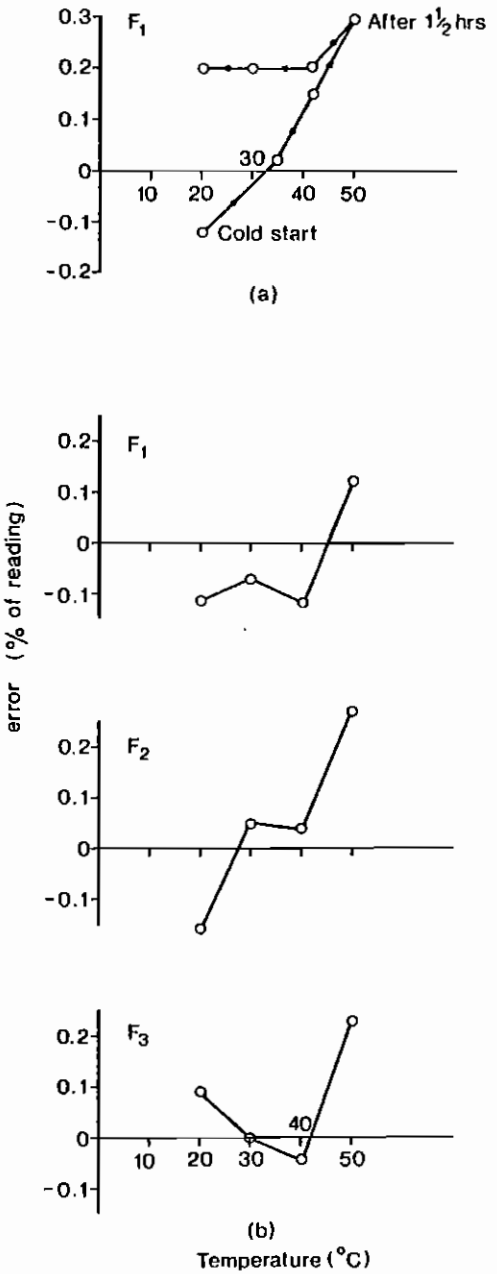
0.3
0.2
0.1
0
-0.1
-0.2
F1
After 1½ hrs
30
10
20
40
50
Cold start
(a)
error (% of reading)
F1
F2
F3
40
(b)
Temperature (°C)

Fig. 8

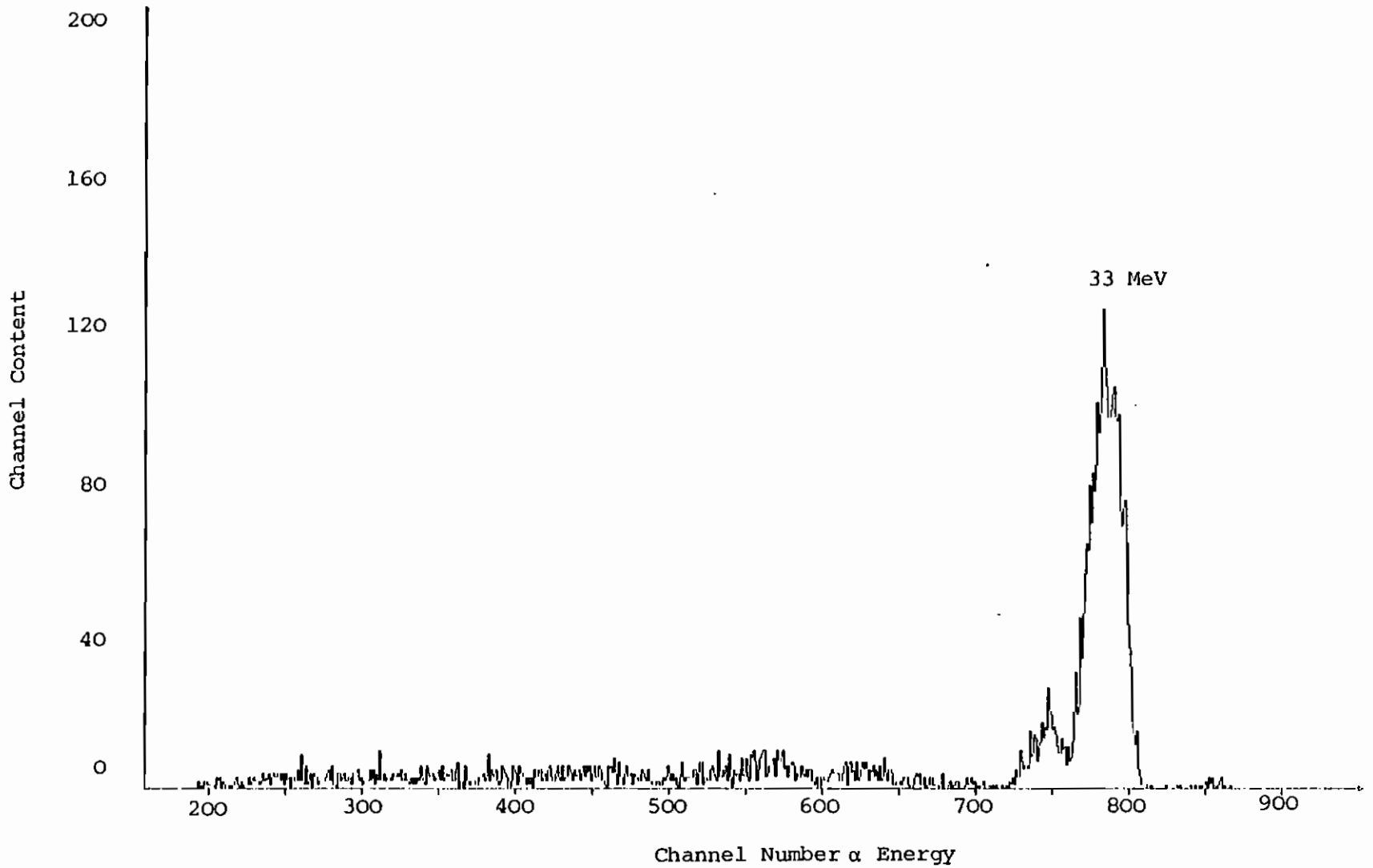
200
160
120
80
40
0
Channel Content
33 MeV
200
300
400
500
600
700
800
900
Channel Number α Energy

Fig. 9

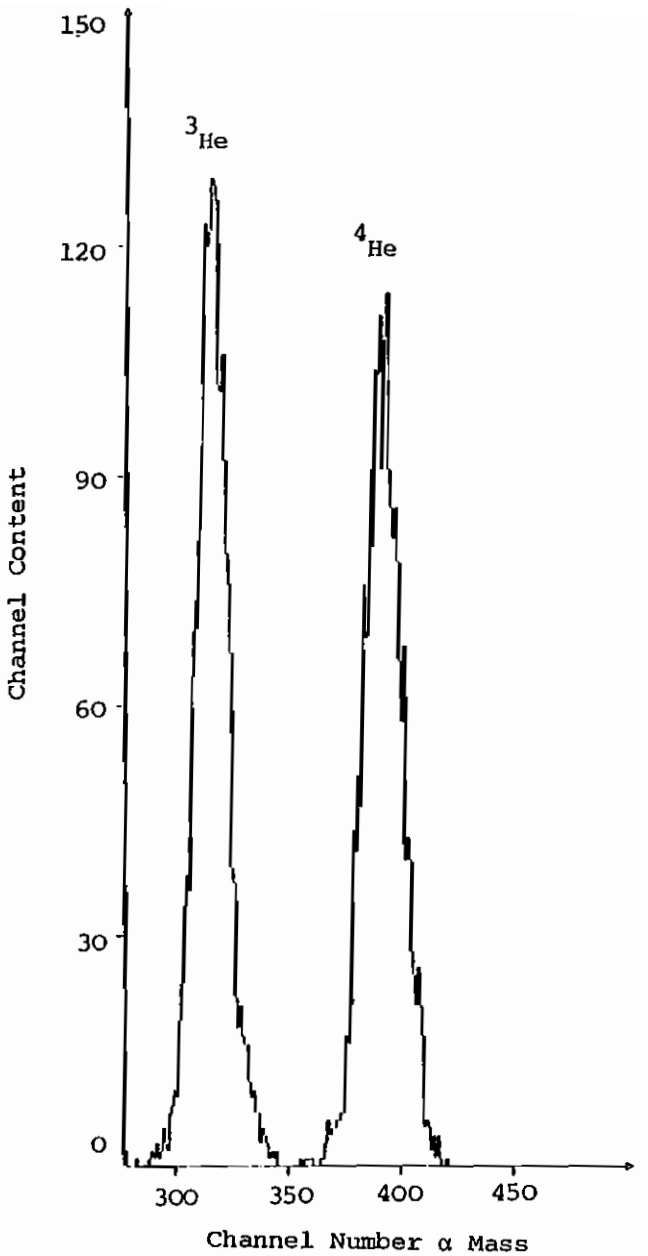
150
120
90
60
30
0
Channel Content
^{3}He
^{4}He
300
350
400
450
Channel Number α Mass

Fig. 10

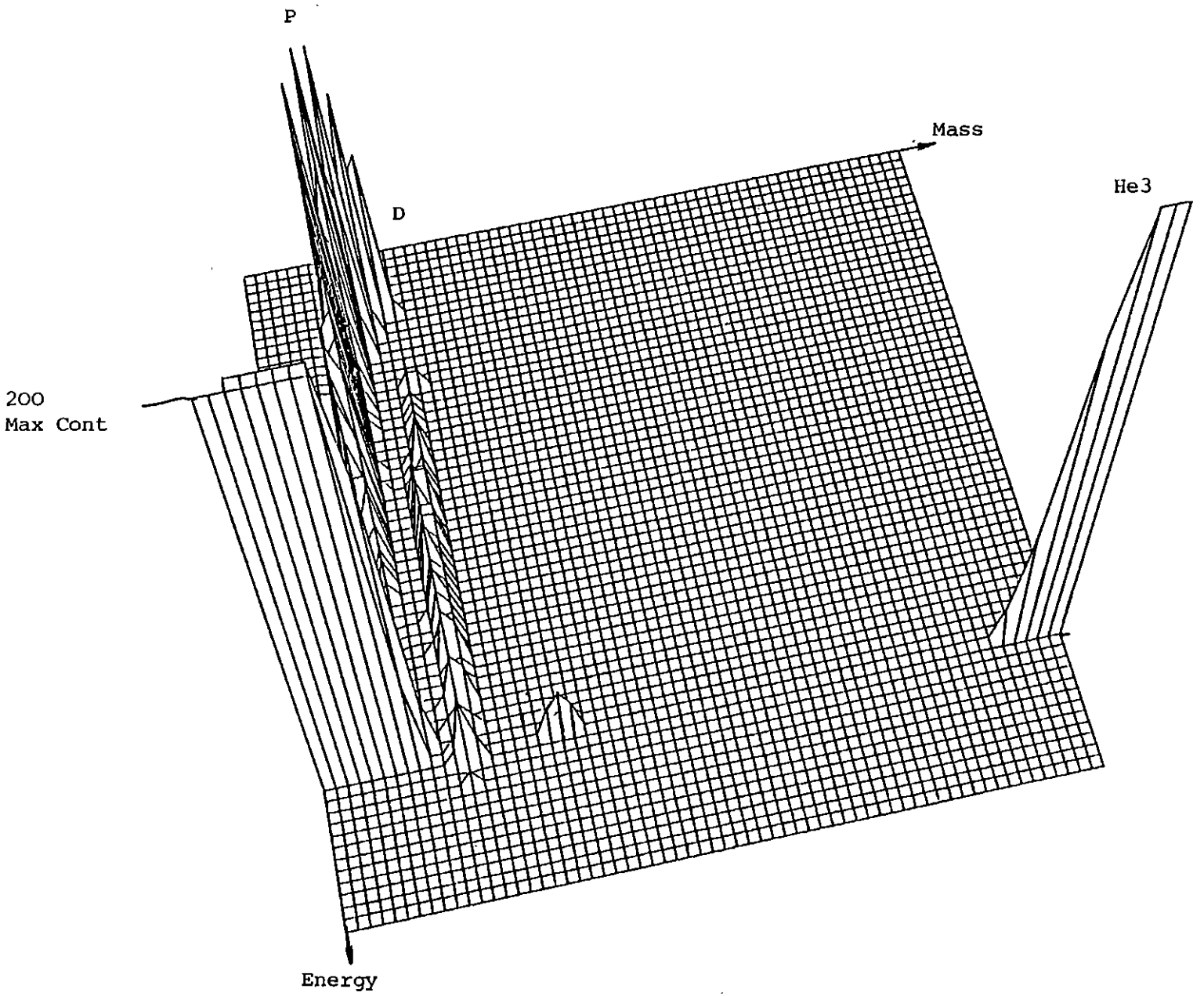

Fig. 11

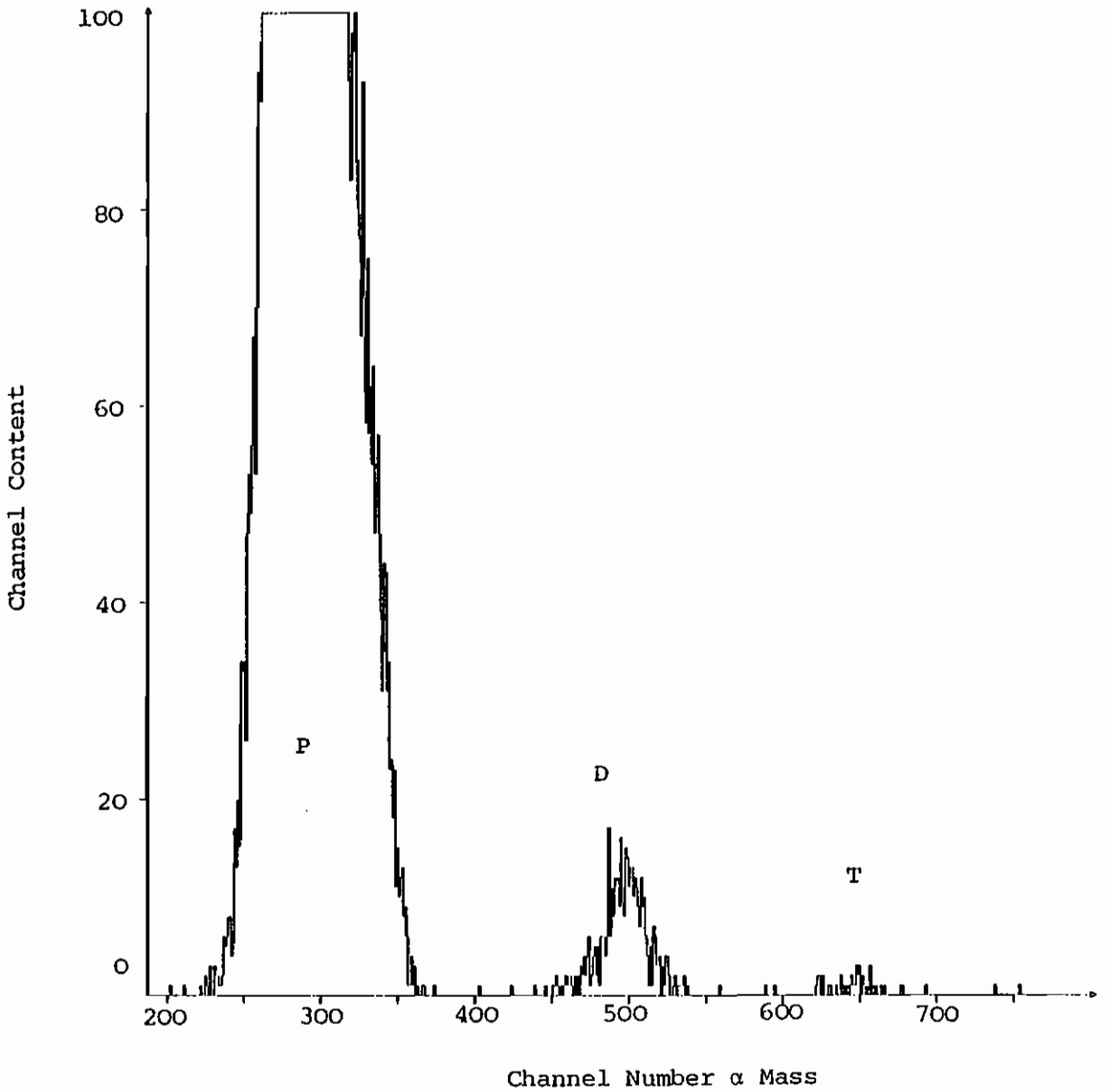
100
80
60
40
20
0
Channel Content
P
D
T
200
300
400
500
600
700
Channel Number α Mass

Fig. 12

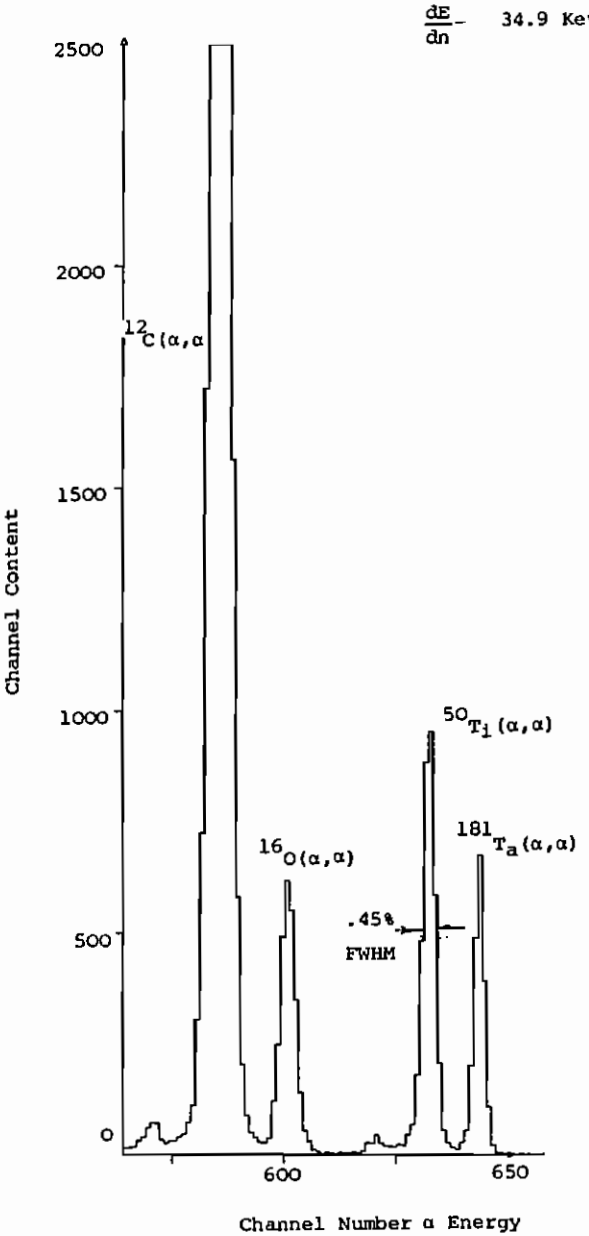
dE/dn = 34.9 Kev/channel
2500
2000
1500
1000
500
0
Channel Content
12C(α,α
16O(α,α)
50Ti(α,α)
181Ta(α,α)
.45%
FWHM
600
650
Channel Number α Energy

Fig. 13

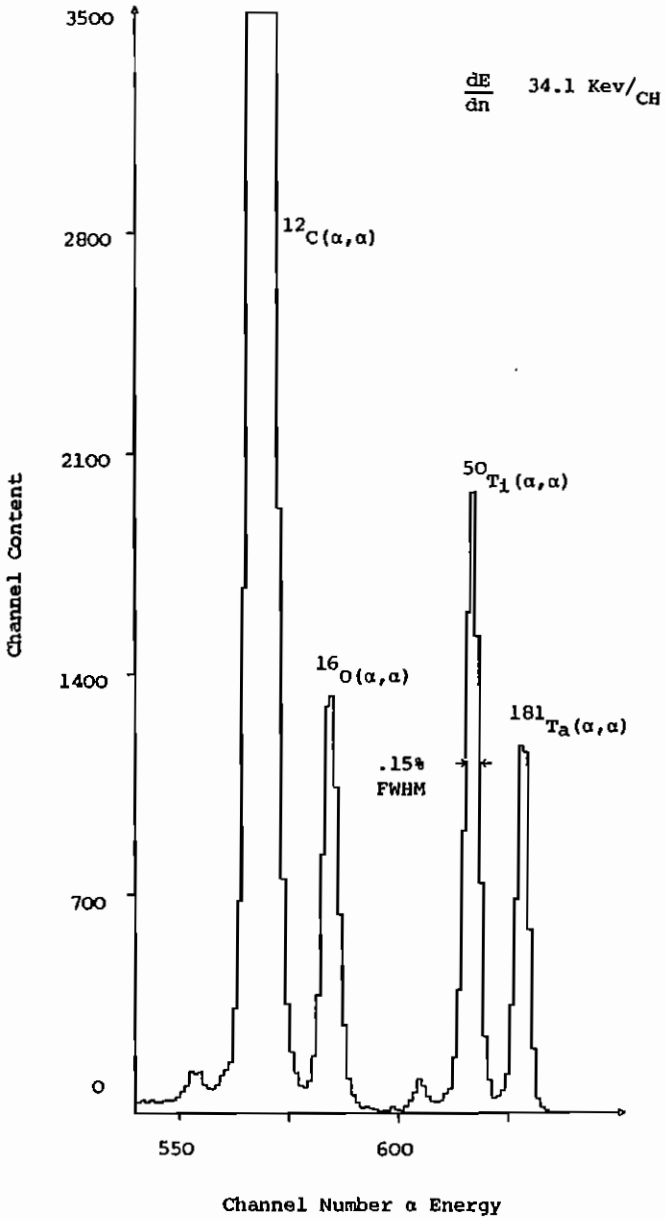
3500
2800
2100
1400
700
0
Channel Content
dE/dn 34.1 Kev/CH
12C(α,α)
16O(α,α)
50Ti(α,α)
181Ta(α,α)
.15% FWHM
550
600
Channel Number α Energy

Fig. 14

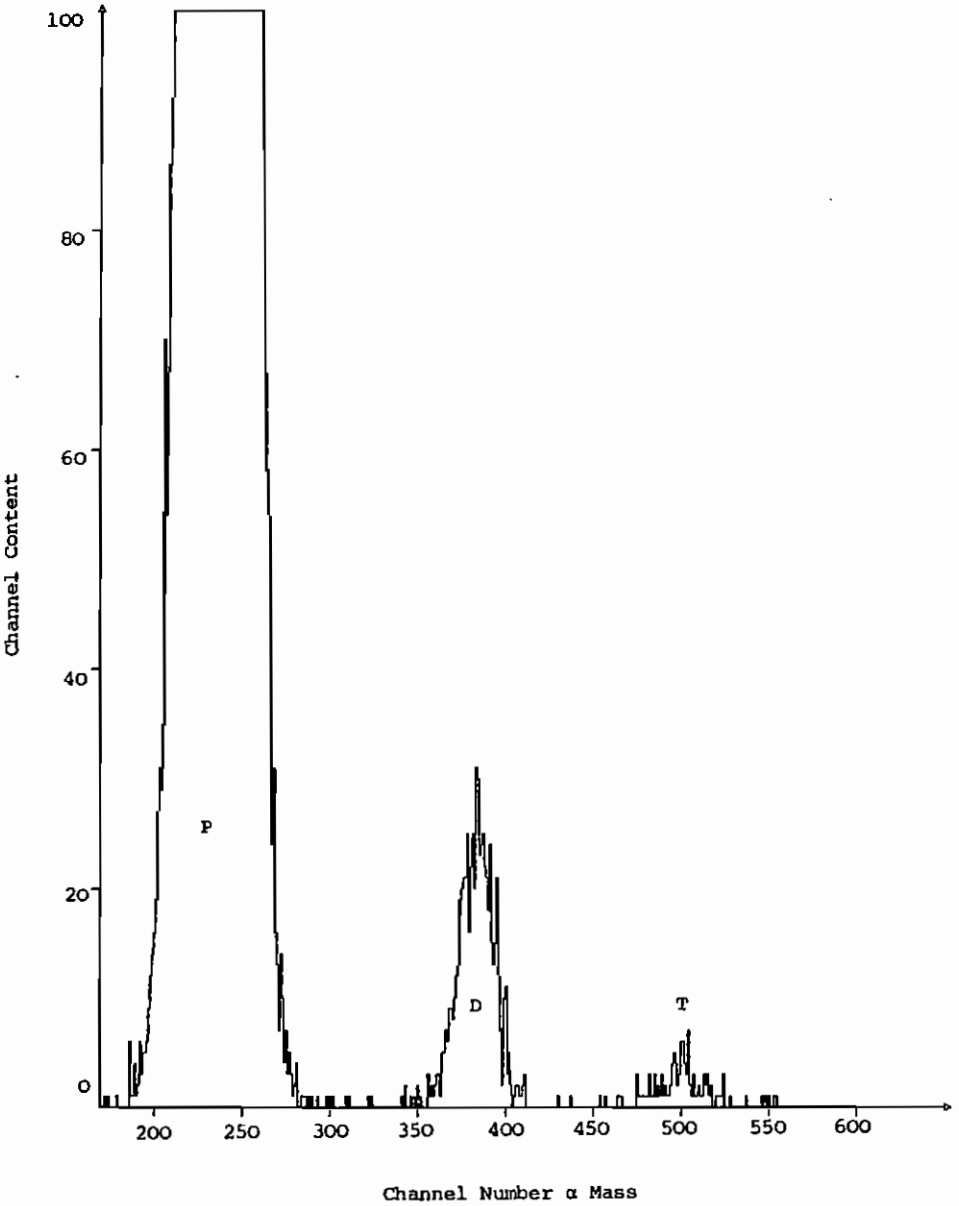
100
80
60
40
20
0
Channel Content
P
D
T
200
250
300
350
400
450
500
550
600
Channel Number α Mass

Fig. 15